33RD INTERNATIONAL COSMIC RAY CONFERENCE, RIO DE JANEIRO 2013
THE ASTROPARTICLE PHYSICS CONFERENCE

A search for Neutrino Emission from the Fermi Bubbles with the ANTARES Telescope

V. KULIKOVSKIY[1,2,3] FOR THE ANTARES COLLABORATION.

[1] *INFN Sezione di Genova, via Dodecaneso 33, Genoa, Italy*
[2] *APC, Université Paris Diderot, CNRS/IN2P3, CEA/IRFU, Observatoire de Paris, Sorbonne Paris Cité, 75205 Paris, France*
[3] *SINP MSU, Vorobyevi gory, 1, Moscow, Russia*

vladimir.kulikovskiy@ge.infn.it

Abstract: Analysis of the Fermi-LAT data has revealed two extended structures above and below the Galactic Centre emitting gamma rays with a hard spectrum, the so-called Fermi bubbles. Some of the promising explanations of this phenomenon assume that accelerated cosmic rays interact with an interstellar medium in the Fermi bubble regions producing pions. Gamma rays and high-energy neutrinos are expected with similar flux from the pion decay. The ANTARES detector is a neutrino telescope located in the Mediterranean Sea, a geographical position which enables good visibility to the Fermi bubble regions. Using ANTARES data from 2008 to 2011 upper limits on the neutrino flux for $E_\nu > 5$ TeV from the Fermi bubbles were derived for various assumed energy cutoffs of the source. No statistically significant excess of events was observed using data corresponding to 3.5 years of lifetime.

Keywords: Fermi bubbles, neutrino, astronomy, astroparticle.

1 Fermi bubbles

Analysis of data collected with the Fermi-LAT experiment has revealed two large spherical structures centred around our Galactic Centre and perpendicular to the galactic plane — the so-called Fermi bubbles [1]. These structures are characterised by gamma-ray emission with a hard E^{-2} spectrum and a relatively constant intensity over the full emission region. The approximate edges of the Fermi bubble regions seen in gamma rays using the Fermi-LAT data are shown in figure 1. The size of the simplified shape shown in the same figure is 0.66 sr.

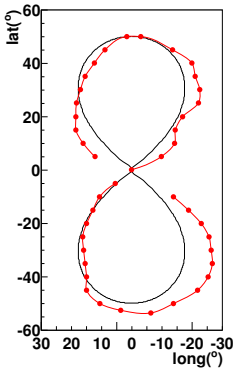

Figure 1: Approximate edges (red line, circles) of the north and south Fermi bubbles respectively in galactic coordinates identified from the 1–5 GeV maps built from the Fermi-LAT data [1]. The contour line is discontinuous at the region of the Galactic Centre as the maps are severely compromised by the poor subtraction and interpolation over a large number of point sources in this region. Simplified shape of the Fermi bubles used in this analysis (black line).

Signal from the Fermi bubble regions was also observed in the microwave band by WMAP [2], in the X-rays by ROSAT [3] and, recently, in the radio-wave band [4]. Several proposed models explaining the emission include hadronic mechanisms, in which gamma rays together with neutrinos are produced by the collisions of cosmic-ray protons with very underdense interstellar matter [5, 6, 7]. Other types of the models exclude the neutrino emission or assume lower fluxes. The observation of a neutrino signal from the Fermi bubble regions may play an unique role in discriminating between models.

The estimated photon flux in the energy range 1–100 GeV covered by the Fermi-LAT detector from the Fermi bubble regions is [1]:

$$E^2 \mathrm{d}\Phi_\gamma/\mathrm{d}E \approx 3-6\times10^{-7}\,\mathrm{GeV\,cm^{-2}\,s^{-1}sr^{-1}} \qquad (1)$$

Assuming a hadronic model in which the gamma-ray and neutrino fluxes arise from the decay of neutral and charged pions respectively, the ν_μ and $\overline{\nu}_\mu$ fluxes are proportional to the gamma-ray flux and their proportionality coefficients are about 0.211 and 0.195 correspondingly [8]. With this assumption and using Equation (1):

$$E^2 \mathrm{d}\Phi_{\nu_\mu+\overline{\nu}_\mu}/\mathrm{d}E \equiv A_{\mathrm{theo}}, \qquad (2)$$

$$A_{\mathrm{theo}} \approx 1.2-2.4\times10^{-7}\,\mathrm{GeV\,cm^{-2}\,s^{-1}sr^{-1}}, \qquad (3)$$

the extrapolation of Equation (2) towards higher energies can be represented by:

$$E^2 \mathrm{d}\Phi_{\nu_\mu+\overline{\nu}_\mu}/\mathrm{d}E \approx A_{\mathrm{theo}} \mathrm{e}^{-E/E_\nu^{\mathrm{cutoff}}}. \qquad (4)$$

The neutrino flux, as well as the gamma-ray flux, is expected to have an exponential energy cutoff represented in equation 4 by E_ν^{cutoff}. The cutoff is determined by the primary protons which have a suggested cutoff E_p^{cutoff} in the range 1–10 PeV [5]. The corresponding neutrino-energy

cutoff may be estimated by assuming that the energy transferred from p to ν derives from the fraction of energy going into charged pions ($\sim 20\%$) which is then distributed over four leptons in the pion decay. Thus:

$$E_\nu^{\rm cutoff} \approx E_p^{\rm cutoff}/20, \quad (5)$$

which gives a range 50–500 TeV for $E_\nu^{\rm cutoff}$.

2 The ANTARES neutrino telescope

The ANTARES telescope is a deep-sea Cherenkov detector which is located 40 km from Toulon at a mooring depth of 2475 m. The energy and direction of incident neutrinos are measured by detecting the Cherenkov light produced in water from muons originating in the charged-current interactions of ν_μ and $\bar{\nu}_\mu$. The light is detected with a three-dimensional array of 885 optical modules, each containing a 10 inch PMT. More details on the detector construction, its positioning system and the time calibration can be found in [9, 11, 10].

The ANTARES detector started data-taking with the first 5 lines installed in 2007. The full detector was completed in May 2008 and has been operating continuously ever since.

Not the only neutrinos produced by the cosmic sources present the events in the detector. Cosmic rays produce particle showers when interacting with the atmosphere. Muons and neutrinos created in these atmospheric showers provide two main background components for the search for cosmic neutrinos. The more than 2 km of water above the detector act as a partial shield against the atmospheric muons. Below the detector is protected by the Earth. As the downgoing atmospheric muon background at these depths is still bigger than the expected signal, only upgoing events can be used for the cosmic signal search. The ANTARES neutrino telescope, located in the Northern Hemisphere, has an excellent visibility by means of the upgoing neutrinos to the Fermi bubbles. Atmospheric neutrinos may traverse the Earth and lead to upward-going tracks in the detector, presenting an irreducible background. The signal-to-noise ratio can be improved by rejecting low-energy neutrino events as the spectrum of the atmospheric neutrinos is expected to be steeper than the expected source spectrum.

Tracks are reconstructed using the arrival time of the photons together with the positions and directions of the photomultipliers. Details of the tracking algorithm are given in [12]. Only events reconstructed as upgoing have been selected for this analysis. In addition, cuts on the reconstruction quality parameters have been applied in order to reject downgoing atmospheric muon events that are incorrectly reconstructed as upgoing tracks. These parameters are the quality Λ of the track fit which is derived from the track fit likelihood and the uncertainty β of the reconstructed track direction. Simulations for an E^{-2} neutrino-energy spectrum yield a median angular resolution on the neutrino direction of less than 0.6° for the events with $\Lambda > -5.2$ and $\beta < 1^o$.

A shower-like events can be identified by using the second tracking algorithm with a two χ^2-like fits of each event, assuming the hypothesis of a relativistic muon ($\chi^2_{\rm track}$) and that of a shower-like event ($\chi^2_{\rm point}$) [13]. Events with $\chi^2_{\rm track} > \chi^2_{\rm point}$ were excluded from the analysis.

In this analysis the energy was estimated using Artificial Neural Networks [14]. The used parameters include the number of detected photons and the total deposited charge. The median energy resolution is roughly 50% for neutrinos with an energy of 10 TeV.

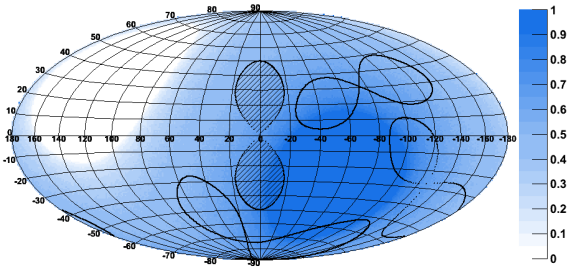

Figure 2: Visibility of the sky at the ANTARES site in galactic coordinates. Maximum corresponds to a 24 h per day visibility. The area of the Fermi bubbles (on-zone) is in the centre. The regions corresponding to the three off-zones around the maximum of the visibility are also depicted.

3 Analysis

Data in the period from May 2008, when the detector started to operate in its complete configuration, till December 2011 were used. In total 806 days were selected for the analysis. A signal from the Fermi bubbles was searched for by comparing the number of selected events from this area (on-zone) with this in comparable regions with no expected signal (off-zones). The simplified shape of the Fermi bubbles used in this analysis is shown in Figure 1. The events selection was based on two parameters, namely the track quality parameter $\Lambda^{\rm cut}$ and the reconstructed energy $E^{\rm cut}_{\rm Rec}$. The reconstructed energy was used to decrease the atmospheric neutrino background while Λ was used mostly to remove the atmospheric muons. The analysis adopted a blinding strategy in which the cut optimisation was performed using simulated data for the signal and the events arriving from the off-zones for the background.

Off-zones with the same size and shape as the on-zone were defined using events coming from the same solid angle in local coordinates as the on-zone events, but shifted with some fixed delay in time. This ensures the same expected number of background events, as their number is proportional to the efficiency of the detector, which is a function of the local coordinates only. The off-zones defined in this way are fixed in the sky. The size of the Fermi bubbles allows to select at maximum three non overlapping off-zones. The Fermi bubble regions and the three off-zones are shown in figure 2 together with the sky visibility. The visibility to each point on the sky was calculated as a part of the sidereal day during which it is below the horizon (in order to produce upgoing events in the detector). The visibility to each zone is 0.68 (0.57 for the northern part and 0.80 for the southern part of the Fermi bubble regions).

The difference in the number of background events between the on-zone and the three off-zones was tested. Firstly, the number of events in the off-zones was extracted from the data for various cuts (Λ, $E_{\rm Rec}$) and the difference in the event numbers between each pair of off-zones was calculated. This difference was compared with the statistical uncertainty and no deviation was seen beyond the expected statistical fluctuations. Secondly, the number of events in the

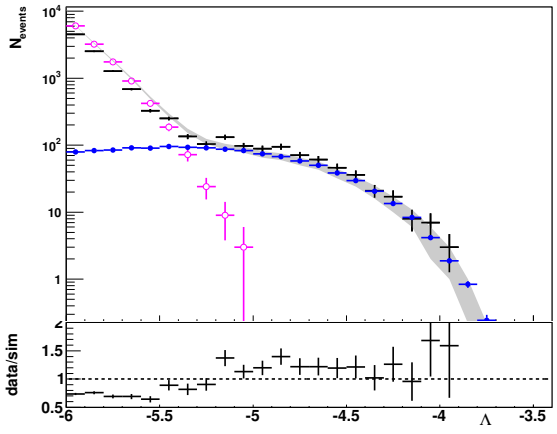

Figure 3: Distribution of the fit-quality parameter Λ for the upgoing events arriving from the three off-zones: data (black crosses), 64% confidence area given by the total background simulation (grey area), $\nu_{\rm atm}^{\rm sim}$ (blue full cirles), $\mu_{\rm atm}^{\rm sim}$ (pink empty circles); bin-ratio of the data to the total background simulation (bottom).

on-zone together with the average number of events in the three off-zones was tested using the simulated atmospheric background and the difference was found to be within the expectation from the statistical uncertainty.

The simulation chain for ANTARES is described in [15]. For the expected signal from the Fermi bubbles the flux according to equation 4 was assumed. Four different cutoffs $E_{\rm cut}^{\nu}$ were considered in this analysis: no cutoff ($E_{\nu}^{\rm cutoff}=\infty$), 500 TeV, 100 TeV and 50 TeV which correspond to the suggested cutoff of the proton spectrum. Atmospheric neutrinos were simulated using the model from the Bartol group [16] which does not include the decay of charmed particles. At energies above 100 TeV the semi-leptonic decay of short-lived charmed particles might become a significant source of atmospheric neutrino background. The uncertainty introduced by the estimation of this flux contribution ranges over several orders of magnitude. Due to the comparison of on and off zones and the final cut ~ 10 TeV (defined in the end of this section) the flux from the charmed particle decay does not have a significant impact on the analysis nor alter the final result on upper limits.

Figure 3 shows the distribution of data and simulated events as a function of the parameter Λ for events arriving from the three off-zones. Here the events with at least 10 detected photons associated with the reconstructed track were selected with the requirement of angular error estimate $\beta < 1^{\circ}$. The latter condition is necessary in order to ensure a high angular resolution to avoid events originating from the off-zone region being associated with the signal region and vice versa. The requirement on the number of photons removes most of the low-energy background events.

Figure 3 shows a change of the main background component at $\Lambda \sim -5.35$: for $\Lambda < -5.35$ most of the events are misreconstructed atmospheric muons while for $\Lambda > -5.35$ the upgoing neutrino events are dominant. The flux of atmospheric neutrinos in the simulation is 23% lower than observed in the data. This is well within the systematic uncertainty on the atmospheric neutrino flux and the simulation was scaled accordingly in the further analysis.

Table 1: Optimisation results for each cutoff of the neutrino energy spectrum. Average upper limits on the flux coefficient $\overline{A}_{90\%}$ are presented in units of $10^{-7}\,{\rm GeV\,cm^{-2}\,s^{-1}sr^{-1}}$. Bold numbers highlight the cut used for the $\overline{A}_{90\%}$ calculation presented in the last row of the table.

$E_{\nu}^{\rm cutoff}$ (TeV)	∞	500	100	50
$\Lambda^{\rm cut}$	-5.16	-5.14	**–5.14**	–5.14
$\log_{10}(E_{\rm Rec}^{\rm cut}[{\rm GeV}])$	4.57	4.27	**4.03**	3.87
$\overline{A}_{90\%}$	2.67	4.47	8.44	12.43
$\overline{A}_{90\%}^{100}$ (100 TeV cuts)	3.07	4.68	8.44	12.75

Table 1 reports the optimal cuts ($\Lambda^{\rm cut}$, $E_{\rm Rec}^{\rm cut}$) obtained for the four chosen cutoff energies (50, 100, 500 TeV and ∞) of the neutrino source spectrum and the corresponding value of the average upper limit on the flux coefficient $\overline{A}_{90\%}$. Additionally, the optimal cuts for $E_{\nu}^{\rm cutoff}=100$ TeV were applied for the other neutrino-energy cutoffs. The values $\overline{A}_{90\%}^{100}$ are reported for comparison. As the obtained values $\overline{A}_{90\%}$ and $\overline{A}_{90\%}^{100}$ for each cutoff are similar, the 100 TeV cut was chosen for the final event selection.

4 Results

The final event selection with the cut $\Lambda > -5.14$, $\log_{10}(E_{\rm Rec}[{\rm GeV}]) > 4.03$ was applied to the unblinded data. In the three off-zones the average number of background events $\overline{n}_{\rm bg} = (9+12+12)/3 = 11$ was observed. $N_{\rm obs} = 16$ events were measured in the Fermi bubble regions. A significance 1.2 σ as a standard deviation of the no-signal hypothesis was obtained using the method by Li & Ma [19].

The distribution of the energy estimator for both the on-zone and the average of the off-zones is presented in figure 4. A small excess of high energy events in the on-zone is seen with respect to both the average from the off-zones and atmospheric neutrino simulation. In addition, no evident clusters were observed by plotting events seen in the Fermi bubble regions.

Upper limits on the number of signal events were calculated applying a Bayesian approach at 90% C.L. using the probability distrubution with two Poisson distributions for the measurements in the on-zone and in the three off-zones. In order to account for systematic uncertainties in simulations of the signal a special study was performed in which the assumed absorption length in seawater was varied by $\pm 10\%$ and the assumed optical module efficiency varied by $\pm 10\%$. For each variation the number of events was calculated for each cutoff and compared with the value $s_{\rm sim}$ obtained using the standard simulation. The differences were calculated and summed in quadrature to obtain $\sigma_{\rm sim}$. A Gaussian distribution of the efficiency coefficient for the signal with mean $s_{\rm sim}$ and sigma $\sigma_{\rm sim}$ was added to the probability distribution.

The frequentist approach from [18] was used for a cross-check. The statistical uncertainty in the background and the efficiency uncertainty given by signal simulations were used. The results are summarised in Table 2 and are shown in figure 5 .

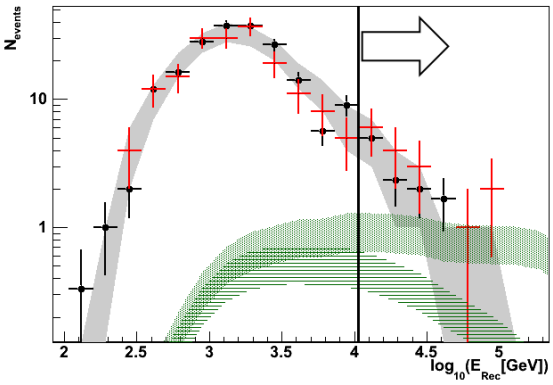

Figure 4: Distribution of the reconstructed energy of the events after the final cut on Λ: events in on-zone (red crosses), average over off-zones (black circles), 64% confidence area given by the total background simulation (grey area), expected signal from the Fermi bubbles without neutrino-energy cutoff (green area filled with dots) and 50 TeV cutoff (green area filled with horizontal lines). Black line with an arrow represents the final event selection.

Table 2: 90% C.L. upper limits on the neutrino flux coefficient A for the Fermi bubbles presented in units of $10^{-7}\,\mathrm{GeV\,cm^{-2}\,s^{-1}\,sr^{-1}}$.

E_ν^{cutoff} (TeV)	∞	500	100	50
s_{sim}	2.9	1.9	1.1	0.7
σ_{sim}, %	14	19	24	27
$A_{90\%}^{\mathrm{upper}}$	5.4	8.7	17.0	25.9
$A_{90\%}^{\mathrm{upper}}$ from [18]	5.9	9.1	16.7	26.4

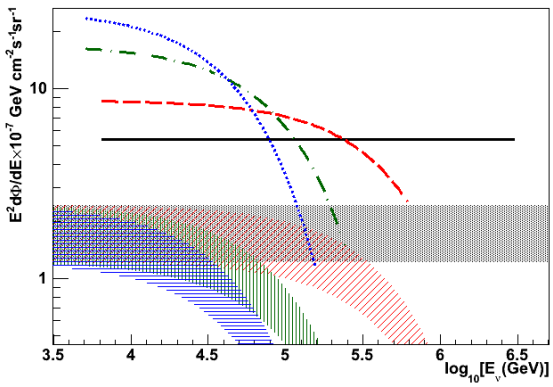

Figure 5: Upper limits on the neutrino flux from the Fermi bubbles, estimated with Bayes' method for different cutoffs: no cutoff (black solid), 500 TeV (red dashed), 100 TeV (green dot-dashed), 50 TeV (blue dotted) together with the theoretical predictions for the case of a pure hadronic model (the same colours, areas filled with dots, inclined lines, vertical lines and horizontal lines correspondingly).

5 Conclusions

High-energy neutrino emission from the region of the Fermi bubbles has been searched for using data from the ANTARES detector.

An analysis of the 2008–2011 ANTARES data yielded a 1.2 σ excess of events in the Fermi bubble regions, compatible with the no-signal hypothesis. For the optimistic case of no energy cutoff in the flux, the limits are within a factor of three of a pure hadronic model. The sensitivity will improve as more data is accumulated (more than 65% gain in the sensitivity is expected once 2012–2016 data is added to the analysis). The next generation KM3NeT neutrino telescope [20] will provide more than an order of magnitude improvement in sensitivity.

Acknowledgment: The authors acknowledge the financial support of the funding agencies: Centre National de la Recherche Scientifique (CNRS), Commissariat á l'Énergie Atomique et aux Énergies Alternatives (CEA), Agence National de la Recherche (ANR), Commission Européenne (FEDER fund and Marie Curie Program), Région Alsace (contrat CPER), Région Provence-Alpes-Côte d'Azur, Département du Var and Ville de La Seyne-sur-Mer, France; Bundesministerium für Bildung und Forschung (BMBF), Germany; Istituto Nazionale di Fisica Nucleare (INFN), Italy; Stichting voor Fundamenteel Onderzoek der Materie (FOM), Nederlandse organisatie voor Wetenschappelijk Onderzoek (NWO), the Netherlands; Council of the President of the Russian Federation for young scientists and leading scientific schools supporting grants, Russia; National Authority for Scientific Research (ANCS-UEFISCDI), Romania; Ministerio de Ciencia e Innovación (MICINN), Prometeo of Generalitat Valenciana and MultiDark, Spain; Agence de l'Oriental, Morocco. Technical support of Ifremer, AIM and Foselev Marine for the sea operation and the CC-IN2P3 for the computing facilities is acknowledged.

References

[1] M. Su, T. Slatyer, D. Finkbeiner, Astrophys. J. 724 (2010) 1044.
[2] G. Dobbler, arXiv:1109.4418v2 [astro-ph.GA], 2011.
[3] S.L. Snowden et al., ApJ 485 (1997)125.
[4] E. Carretti et al., Nature 493(2013) 66.
[5] R.Crocker, F.Aharonian, Phys. Rev. Lett. 106 (2011) 101102.
[6] B. C. Lacki, arXiv:1304.6137 [astro-ph.HE] 2013.
[7] S. Thoudam, arXiv:1304.6972 [astro-ph.HE] 2013.
[8] F.L.Villante, F.Vissani, Phys.Rev. D 78, 103007 (2008).
[9] ANTARES Collaboration, J.A. Aguilar et al., Nucl. Instrum. Meth. A 656 (2011) 11-38 doi:10.1016/j.nima.2011.06.103. See also A. Kouchner, for the ANTARES collaboration, this conference.
[10] ANTARES Collaboration, J.A. Aguilar et al., Astropart. Phys. 34 (2011) 539.
[11] ANTARES Collaboration, S. Adrián-Martínez et al., JINST 7 (2012) T08002.
[12] ANTARES Collaboration, S. Adrián-Martínez et al., ApJ 760 (2012) 53.
[13] ANTARES Collaboration, J.A. Aguilar et al., Astropart. Phys. 34 (2011) 652-662.
[14] J.Schnabel, Nucl. Instrum. Meth. A, NIMA55282, doi:10.1016/j.nima.2012.12.109.
[15] Brunner, J. 2003, in VLVnT Workshop (Amsterdam), ANTARES simulation tools, ed. E. de Wolf (Amsterdam:NIKHEF), `http://www.vlvnt.nl/proceedings.pdf`.
[16] Bartol group, V. Argawal et al., Phys. Rev. D, 53 (1996) 1314-1323.
[17] G.C. Hill and K. Rawlins, Astropart. Phys. 19 (2003) 393-402.
[18] J. Conrad et al., Phys. Rev. D. 67 012002 (2003).
[19] T. Li, Y. Ma, Astrophys. J. 272 (1983) 317-323.
[20] KM3NeT Collaboration, S. Adrián-Martínez et al., Astropart. Phys., 42 (2013) 7-14. See also R.Coniglione et al., for the KM3NeT collaboration, this conference.